Paper No. 143

Seismic test of building floor isolation using polynomial friction pendulum isolators

Lyan-Ywan Lu[1], Liang-Wei Wang[2], Chun-Chung Tsai[3]

ABSTRACT

Compared to structural base isolation, floor isolation is a more cost-effective and efficient means for seismic protection of vibration-sensitive equipment in a building structure. However, in order to protect the precision equipment, floor isolation usually has to satisfy more stringent isolation performance than that of base isolation; at the meantime, it also calls for less isolation displacement demand due to the indoor space limitation. In order to satisfy these multiple demands, in this study, a multi-functional floor isolation system (FIS) that consists of several variable-stiffness sliding isolators, called polynomial friction pendulum isolators (PFPIs), is proposed and studied. Due to its variable-stiffness nature, the proposed system is able to achieve the desired dual performance objectives that were selected during the design stage for two-level seismic loads. The variable-stiffness hysteretic property of the proposed system was verified by a shaking table test conducted on a prototype PFPI-FIS. Moreover, by using the parameters of the prototype system, the seismic performance of the prototype PFPI-FIS under ten ground motions, which represent earthquakes with different spectral contents and intensity levels, are investigated numerically. The simulated results demonstrate that the isolation performance of the PFPI-FIS does comply with the designated dual performance objectives, which yield either acceleration or displacement control depending on the earthquake intensity and isolator drift.

Keywords: *Floor isolation, multi-functional isolator, variable stiffness, pendulum isolator, polynomial function, performance design.*

1. INTRODUCTION

The task of providing seismic protection for interior equipment or non-structural components is important, because the damage of these components may cause operational interruptions of critical facilities or buildings. Relevant research also indicates that attaching vibration-sensitive equipment to the structural floor may prevent the problems of overturning and excessive displacement, but it fails to mitigate the seismic excitation that is usually magnified by the dynamic effect of the underlying structure and can cause serious damage to the equipment (Achour et al., 2011). Seismic isolation which uncouple isolated object from the sources of excitation may provide an effective solution to reduce the amplification of seismic force transmitted to sensitive equipment. Among many kinds of isolation technologies, the floor isolation, where the isolation layer is placed between a raised-floor (a secondary floor system) and the structural floor, can be the most cost-effective method, since it is able to isolate groups of equipment from seismic excitations.

[1] Corresponding author: Professor, Department of Civil Engineering, National Cheng Kung University, 1 University Road, Tainan 701, Taiwan. Email: lylu@mail.ncku.edu.tw, Tel: 886-6-2757575 ex. 63138.

[2] Graduate Student, National Cheng Kung University, Tainan, Taiwan.

[3] Graduate Student, National Kaohsiung First University of Science and Technology, Kaohsiung, Taiwan.

Although seismic isolation is a mature technology, the majority of current studies are associated with structural base isolation. There have been relatively few studies that focus directly on the applications of floor-type isolation (Yang and Agrawal, 2000; Xu et al., 2008).

The application of floor isolation can be a challenging problem, since the seismic protection of precision equipment by a FIS usually calls for a very stringent seismic demand. In particular, the allowable acceleration level for maintaining the integrity of such equipment after an earthquake is usually very low. In order to achieve this strict requirement, a conventional FIS has to adopt a very long isolation period. Consequently, the isolator displacement of the FIS will become excessive in earthquakes of higher intensity. This may further cause isolation bounding problems and lead to severe damage of the isolated equipment and the surrounding structures. On the other hand, due to limitations on interior space, the allowable isolator drift for an FIS is also usually limited. In order to reduce the isolator drift, a conventional FIS has to adopt a shorter isolation period. Consequently, the seismic force transmitted to the isolated equipment may easily exceed the allowable level in a moderate earthquake and thus damage the precision equipment. This is especially true, when the effect of structural dynamic amplification is considered. The above discussions have indicated that the reduction of both the acceleration and displacement responses is needed for a FIS to be successfully implemented. For a conventional FIS, this task is very difficult, if not impossible, to achieve. A variable FIS that possesses multiple isolation performances may provide a possible solution to the above problem (Lu and Hsu, 2013). To develop such a system, this study investigates the usage of a passive variable FIS that primarily consists of several polynomial friction pendulum isolators (PFPIs) installed under a floor system. A PFPI is a type of sliding isolator with variable stiffness (Lu et al., 2011). Because of this variable property, the proposed FIS (hereafter, called PFPI-FIS) has different isolation periods for different isolator displacements.

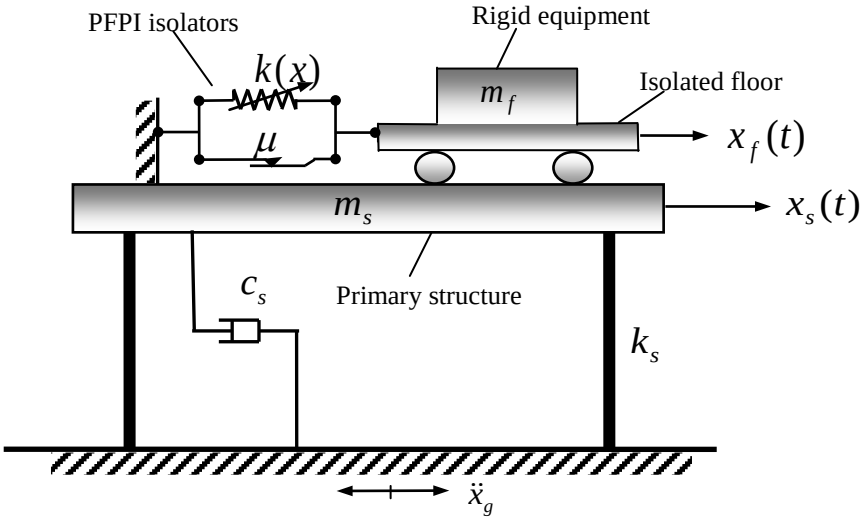

Figure 1. Mathematic model of a building with a PFPI floor-isolation system.

2. FORMULATION OF A STRUCTURE WITH A PFPI FLOOR ISOLATION SYSTEM

2.1 Mathematical Model For Numerical Analysis

The mathematical model of a building with a PFPI-FIS may be shown by Fig. 1. In this 2-DOF model, the symbols $k(x)$ and μ represent the stiffness and friction coefficients of the PFPI isolation system, respectively; $x_f(t)$ and $x_s(t)$ are the relative-to-the-ground displacements of the isolated floor and the primary structure, respectively; $\ddot{x}_g(t)$ denotes the ground acceleration; the symbols m_f and m_s denote the masses of the isolated floor and the primary structure; k_s and c_s represent the stiffness and damping coefficients of the structure. Notably, since the dynamic effect of the equipment is neglected, m_f may include the mass of the equipment. The dynamic

equation of the mathematic model shown in Fig. 1, which combines PFPI-FIS and the primary structure, can be written in a state-space form

$$\dot{\mathbf{z}}(t) = \mathbf{A}\,\mathbf{z}(t) + \mathbf{B}\,u(t) + \mathbf{E}\,\ddot{x}_g(t) \tag{1}$$

where $u(t)$ denotes the total shear force of the PFPI isolation system, while $\mathbf{z}(t)$ and $\mathbf{A}$ are the state vector and the system matrix; and $\mathbf{B}$ and $\mathbf{E}$ denote the placement matrices of the PFPI forces and the ground excitation, respectively. Notably, the force $u(t)$, which is induced by the seismic motion of the underlying structure onto which the FIS is installed, is equivalent to the horizontal seismic force applied on the FIS.

2.2 Shear force components of a PFPI isolator

For a general sliding isolator with variable curvature, Lu et al. (2011) has derived the following formula for computing its shear force

$$u(x) = u_r(x) + u_f(\dot{x}) \tag{2}$$

where $u_r(x)$ and $u_f(x)$ represent the components of the restoring force and the friction force, respectively; while $x(t)$ and $\dot{x}(t)$ denote the isolator displacement and sliding velocity, respectively. Provided that the isolator is in its sliding state, the above two force components can be approximated by

$$u_r(x) = P\,y'(x),\quad u_f(\dot{x}) \approx \mathrm{sgn}(\dot{x})\mu P \quad \text{(for sliding state)} \tag{3}$$

where $y(x)$ is the geometric function of the sliding surface and $y'(x)$ is the derivative. For the PFPI isolators tested in this study, Eq. (3) will be accurate enough to predict their hysteresis loop. If the friction coefficient of the sliding isolators depends on the sliding velocity rather than a constant, the above formulas for the PFPI are still valid, but the friction coefficient μ has to be replaced by $\mu(\dot{x})$. In this study, the renowned Constantinou's friction model (Constantinou, 1990) will be employed to describe the relationship of μ and $\dot{x}$.

Isolator stiffness and period

The secant stiffness $k(x)$ of the PFPI system, commonly used in practice, can be defined by directly dividing the restoring force by the isolator displacement, i.e.,

$$k(x) = \frac{u_r(x)}{x} = \frac{P\,y'(x)}{x} \tag{4}$$

By using this definition, one can further compute the isolation period T of the PFPI system as following

$$T(x) = 2\pi\sqrt{\frac{M}{k(x)}} = 2\pi\sqrt{\frac{P/g}{k(x)}} = 2\pi\sqrt{\frac{x}{g\,y'(x)}} \tag{5}$$

Eq. (4) and (5) state that the isolation stiffness and period of the PFPI are both function of $y'(x)$ and are independent of the isolated floor mass.

3. DESIGN OF PFPI ISOLATORS

3.1 Choosing the geometry of the sliding surface

As shown in Eqs. (3)-(5), the restoring force, stiffness and period of the PFPI system all rely on the geometric function $y(x)$ of the sliding surface; therefore, the desirable mechanical property of the isolation system can be achieved by properly choosing the function $y(x)$. To enable the PFPI to satisfy multiple design objectives, this study defines the geometric function by the following sixth-order polynomial

$$y(x) = (1/6)\,a\,x^6 + (1/4)\,c\,x^4 + (1/2)\,e\,x^2 \tag{6}$$

where a, c and e are three constant coefficients to be determined. Next, using Eq. (6) in Eq. (4) yields a four-order polynomial for the PFPI stiffness, i.e.,

$$\bar{k}(x) = \frac{k(x)}{P} = \frac{y'(x)}{x} = a\,x^4 + c\,x^2 + e \tag{7}$$

where $\bar{k}(x)$ denotes the normalized stiffness with respect to the vertical load P.

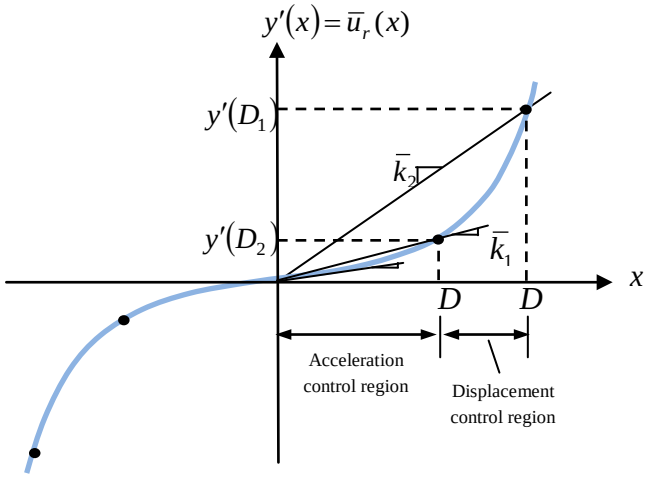

Figure 2 The normalized restoring force of the PFPI.

3.2 Conversion of isolator parameters

From Eq. (7), it is clear that the stiffness of a PFPI isolation system is primarily determined by the three polynomial coefficients a, b and c. In this section, a design procedure that determines their values to satisfy multiple performance objectives will be introduced. Firstly, for the convenience of the design, the three polynomial coefficients, which are purely mathematical, have to be converted into other parameters that have more engineering meaning.

From Eq. (3), it is known that the normalized restoring force $\bar{u}_r(x) = u_r(x)/P$ of the PFPI defined by the sixth-order polynomial in Eq. (6) will be an odd function as depicted in Fig. 2. A curve defined by this odd function will pass through the origin and is anti-symmetric about the origin. The slope of a secant line on the curve is equivalent to the isolator's normalized stiffness $\bar{k}(x)$ defined in Eq. (7). As illustrated in Fig. 2, let $\bar{k}_1$ and $\bar{k}_2$ be the isolator's stiffness at two different isolator displacements D_1 and D_2, respectively; while $\bar{k}_0$ be the tangent stiffness at the origin. Then, we have

$$y''(0) = \bar{k}_0, \quad y'(D_1) = \bar{k}_1 D_1, \quad y'(D_2) = \bar{k}_2 D_2 \tag{8}$$

Next, substituting $y'(x)$ from Eq. (6) in Eq. (7), one may obtain three simultaneous equations for the coefficients a, b and c. The solution of these simultaneous equations leads to

$$a = \frac{-(D_2/D_1)^2(\bar{k}_1 - \bar{k}_0) + (\bar{k}_2 - \bar{k}_0)}{D_1^2 D_2^2[(D_2/D_1)^2 - 1]}, \quad c = \frac{(D_2/D_1)^4(\bar{k}_1 - \bar{k}_0) - (\bar{k}_2 - \bar{k}_0)}{D_2^2[(D_2/D_1)^2 - 1]}, \quad e = \bar{k}_0 \tag{9}$$

Eq. (9) converses the polynomial coefficients a, b, c into the five parameters $\bar{k}_0$, $\bar{k}_1$, $\bar{k}_2$, D_1 and D_2 that are more engineering meaningful than the original coefficients.

Table 1 Design steps and parameters for the prototype PFPIs.

Step	Task	Parameter		Value
1	Decide allowable isolator displacements	First displacement (D_1)		0.08m
		Second displacement (D_2)		0.12m
2	Decide desired isolation periods	Initial period (T_0)		Infinite
		First period (T_1)		3.0 s
		Secon period (T_2)		1.6 s
3	Compute normalized isolator stiffnesses by using Eq. (10)	Initial stiffness ($\bar{k}_0$)		0.0 (1/m)
		First stiffness ($\bar{k}_1$)		0.447 (1/m)
		Second stiffness ($\bar{k}_2$)		1.572 (1/m)
4	Compute polynomial coeffieicents by using Eq. (9)	Polynomial coeffieicents	a	4915.36 ($1/m^5$)
			c	38.39 ($1/m^3$)
			e	0.0 ($1/m$)

3.3 Design procedure and results

To explain how the above five design parameters are determined for the prototype PFPIs used in the experiment, let us first assume that the stiffness $\bar{k}(x)$ of the isolators is increased monotonically along with the increase of the isolator displacement (see Fig. 2). This implies that $\bar{k}_0 < \bar{k}_1 < \bar{k}_2$ ($T_0 > T_1 > T_2$), where $D_1 < D_2$. Furthermore, let D_1 and D_2 be the allowable isolator displacements corresponding to two design earthquakes of a low and a high intensity, respectively, and $\bar{k}_1$ and $\bar{k}_2$ represent the desired isolator stiffness corresponding to D_1 and D_2, respectively. In practice, the two-level earthquakes can be those already defined in many design codes, such as the design basis earthquake (DBE) and maximum considered earthquake (MCE) given in International Building Code (IBC, 2009).

With the above two allowable values of D_1 and D_2 for two different earthquake intensities, the following dual performance objectives can be incorporated into the PFPI design: (1) For the first level (lower-intensity) earthquake, where the isolator displacement is below D_1, the performance objective of the PFPI design is set to protect the isolated object by minimizing its acceleration response (acceleration control). Thus, a longer isolation period should be adopted for T_1 (i.e., smaller $\bar{k}_1$), in order to achieve the first objective. (2) For the second level (higher-intensity) earthquake, where the isolator displacement exceeds D_1 and may become excessive, the performance objective of the PFPI design switches to suppress the isolator displacement, so that the displacement may be restrained within the allowable value D_2 (displacement control). In this case, a shorter isolation period should be adopted for T_2 (i.e., larger $\bar{k}_2$).

With the above dual objectives, a four-step design procedure, which has been used in the

prototype PFPI design, is suggested in Table 1. In step 2, the following conversion may be used.

$$\bar{k}_j = 4\pi^2/(T_j{}^2\, g) \quad (\text{for } j = 0, 1, 2) \tag{10}$$

The last column of Table 1 shows the design values for the prototype PFPIs used in the test. As shown, the first and second periods of the tested PFPI are taken to be $T_1 = 3.0\,\text{s}$ and $T_2 = 1.6\,\text{s}$, while the initial period T_0 is taken to be infinite (i.e., $\bar{k}_0 = 0$), in order to attain a better acceleration reduction result for earthquakes of low intensity.

4. TEST OF A PROTOTYPE PFPI-FIS

To experimentally verify the concept of the PFPI-FIS, a shaking table test for a prototype PFPI-FIS was conducted. The test setup is depicted in Fig. 3, which involved four PFPI bearings mounted under the four corners of a rigid floor system that was simulated by several steel plates with the total mass about $m_f = 1020\,\text{kg}$. A sinusoidal ground displacement with variable amplitude and frequency was also imposed on the PFPI-FIS, so that its isolator displacement could be gradually increased. Fig. 4 depicts the experimental friction coefficient as a function of the sliding velocity for the prototype PFPI-FIS. It is shown in Fig. 4 that the friction coefficient of the PFPIs, whose sliders are composed of Teflon material, is velocity dependent rather than a constant. The velocity-dependent friction property of Teflon materials usually can be well predicted by Constantinou's model (Constantinou, 1990) shown below

$$\mu(t) = \mu_f + (\mu_f - \mu_s)e^{-r|\dot{x}(t)|} \tag{11}$$

where μ_s and μ_f denote the friction coefficients at very-low and very-high sliding velocities. By employing an optimization searching scheme called the generalized pattern search, the optimal parameter values (μ_s, μ_f, r) that best fit the test data in Fig. 4 were identified and listed in Table 2. Using these best-fit parameters, the theoretical friction coefficient for Constantinou's model is also depicted in Fig. 4.

Using the friction coefficients listed in Table 2, Fig. 5 compares the experimental hysteresis loops of the prototype PFPI-FIS with the theoretical ones simulated by using Eq. (2) and (3). Fig. 5 shows that the experimental loops of the PFPI-FIS can be well predicted by Constantinou's model. More importantly, the experimental hysteresis loops also confirm that the PFPI-FIS does possess the desired hysteretic property with variable stiffness, as described in Eq. (2) and (3).

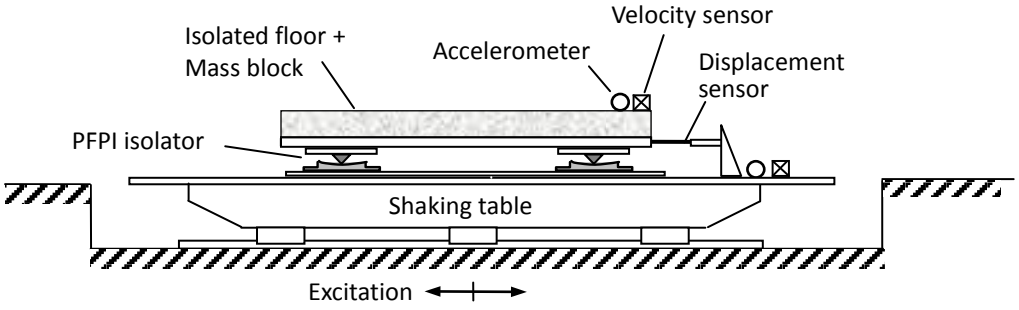

Figure 3 Setup of the hysteresis property test for the prototype PFPI-FIS.

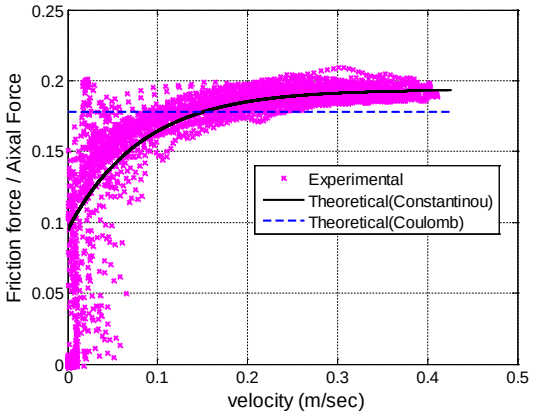

Figure 4 Friction coefficient vs. sliding velocity

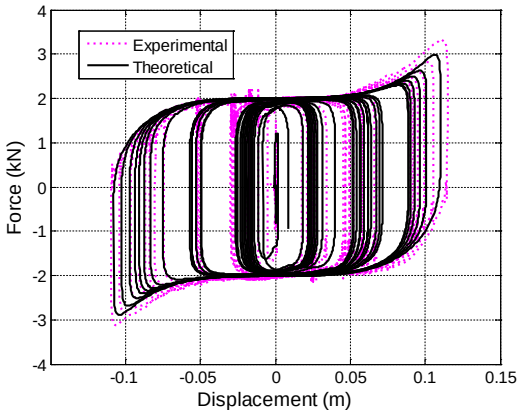

Figure 5 Hysteresis loops of the PFPI-FIS

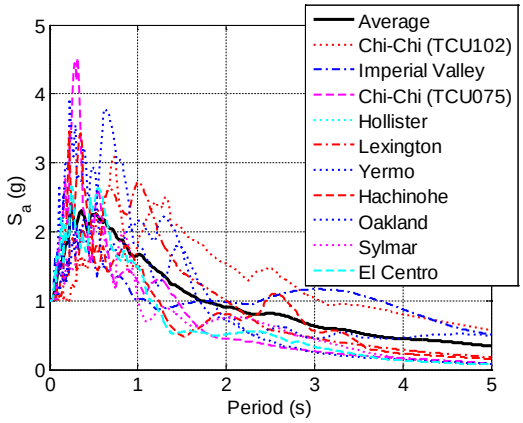

Figure 6 Acceleration response spectra of the selected 10 ground motions (5% damped).

5. NUMERICAL EVALUATION OF ISOLATION PERFORMANCE

In this section, the isolation performance of the prototype PFPI-FIS mounted on a seismic structure will be evaluated numerically. Special attention will be paid to how the system performs under earthquakes with different PGA levels. The parameter values of the PFPI-FIS and the primary structure listed in Table 2, which were identified from the test data, will all be employed throughout the numerical simulation. Ten ground accelerations recorded from ten historical earthquakes with very different spectral characteristics, including near-fault characteristics, will be considered in the numerical study. The 5%-damped normalized acceleration response spectra of these seismic motions are compared in Fig. 6.

Assuming that the tested system is subjected to each of the selected 10 ground motions, Fig. 7 depicts the averages of the PFPI-FIS peak responses for these 10 earthquakes as a function of the PGA level. For the purpose of comparison, two types of FPS floor isolation systems (hereafter, called FPS-FIS) with isolation periods of 3.0s and 1.6s, respectively, are also considered in the figures. These FPS systems intend to represent conventional sliding isolation systems that can only have a constant isolation period. The periods of 3.0s and 1.6s are chosen for these two FPS systems, because they are also the first and second isolation periods (T_1 and T_2) of the PFPI-FIS at the displacements D_1 and D_2. The peak acceleration of a fixed-floor system, representing the case of an un-isolated floor, is also depicted in Fig. 7(a). Moreover, as explained previously, the prototype PFPI system has two design isolator displacements D_1 and D_2, i.e., 0.08m and 0.12m,

respectively (see Table 1). The occurrences of D_1 and D_2, which can be identified in Fig. 7, are marked by blue circles for the PFPI system.

Table 2 Parametric values of PFPI-FIS and primary structure.

Item	Parameter		Value
PFPI - Floor isolation system (from the test)	Isolated floor mass (m_f)		1.02×10^3 kg
	Slider material		Teflon
	Friction coefficients (Contantinous model)	μ_f	0.194 (high-velocity)
		μ_s	0.095 (low-velocity)
		r	0.121 (roundness)
Primary structure (Single DOF)	Strctural members		H shaped steel
	Structural dimention (H×W×D)		4m×3m×2m
	Fundamental period (T_s)		0.36 s
	Fundamental damping ratio (ζ_s)		1.8 %
	Mass of top floor (m_s)		10.25×10^3 kg

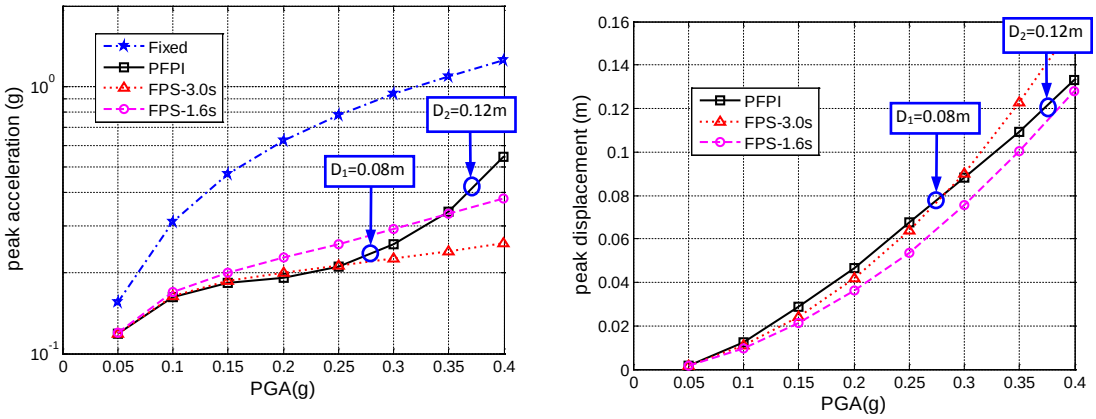

(a) Acceleration of floor systems (b) Isolator displacement

Figure 7 Average peak responses of various floor isolation systems subjected to the selected 10 ground motions.

The following observations can be made from Fig. 7: (1) It is evident in Fig. 7(a) that due to the structural dynamic effect, the peak acceleration of the fixed-floor system is amplified by more than 300% under all PGA levels considered. The figure also demonstrates that all three floor isolation systems (i.e., PFPI, FPS-3.0s, FPS-1.6s) are able to achieve an acceleration reduction rate of more than 60%. (2) For all PGA levels considered, the FPS-3.0s system that may represent a longer-period conventional isolation system has a lower acceleration response but a higher isolator displacement, as compared to the responses of the FPS-1.6s. Generally, for a FPS system, it is difficult to have less acceleration and displacement responses simultaneously. This is also a limitation of a conventional isolation system. (3) For the PFPI system, both Figs. 7(a) and 7(b) demonstrate that the displacement D_1 is a transition point. For an earthquake of lower intensity that results in an isolator displacement less than D_1, the PFPI system performs more like the FPS-3.0s system, which has lower acceleration but higher displacement response. Conversely, for a higher-intensity earthquake that results in a displacement beyond D_1, the isolation behavior of the PFPI system will gradually approach that of the FPS-1.6s, which has lower displacement but higher acceleration response. The peak responses of the PFPI system will be roughly equal to those of the FPS-1.6s, when its isolator displacement is close to D_2, whose corresponding design period is

$T_2 = 1.6$ s. The isolation performance of the PFPI system discussed above is completely consistent with the designated dual design objectives explained previously.

The above dual-performance property may also be observed in time domain. The isolator displacements of the three isolation systems under the Imperial Valley earthquake (PGA=0.4g) are compared in Fig. 8. Because the main shock of this earthquake occurs between 6-8 seconds, the peak responses of all three systems also occur within this time range. Fig. 8 shows that within the period of 6-8 seconds, the PFPI isolator displacement generally exceeds $D_1 = 0.08$ m; therefore, the acceleration and displacement time-histories of the PFPI around its peak responses are closer to those of the FPS-1.6s. On the other hand, after the 8th second, the PFPI responses are reduced, so they become closer to those of the FPS-3.0s. The responses of all three systems are reduced after the 9th second, so their acceleration responses become almost identical.

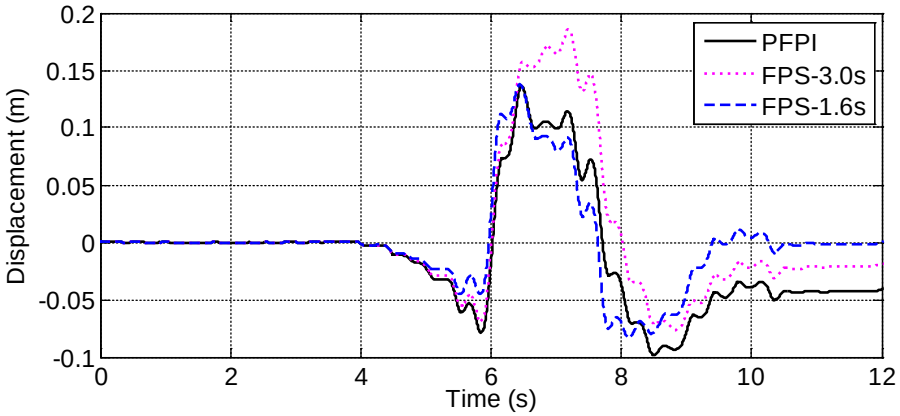

Figure 8 Comparison of isolator displacements (Imperial Valley earthquake, PGA=0.4g).

6. **CONCLUSIONS**

In order to provide better isolation performance, a multi-functional floor isolation system (FIS) that is able to achieve multiple design objectives is proposed and studied both experimentally and numerically in this paper. The proposed system primarily consists of several variable sliding isolators, called polynomial friction pendulum isolators (PFPIs). A PFPI-FIS possesses variable isolation stiffness, so its isolation period is a function of the isolator displacement rather than a constant. This paper evaluates numerically the isolation performance of the PFPI-FIS mounted on the top of a building structure. In the simulation, the system parameters of a prototype PFPI-FIS, which was identified from a shaking table test, was adopted and the seismic responses of the prototype PFPI-FIS subjected to ten ground motions were simulated extensively. The selected ten ground motions represent a wide range of spectral contents and have a gradually increased PGA level. The isolation performance of the PFPI-FIS was also evaluated by comparing its peak responses to those of two conventional floor isolation systems that are compatible with each one of the dual design objectives of the PFPI-FIS. The numerical results demonstrate that the performance of the PFPI-FIS does comply with the designated dual design objectives. In other words, the PFPI-FIS is able to reduce the acceleration response of the isolated floor in an earthquake of a lower PGA level, while the behavior of the PFPI-FIS becomes to suppress the isolator displacement in an earthquake with higher PGA that may result in an excessive isolator drift.

ACKNOWLEDGEMENTS

The authors are grateful to Dr. Pei-Yang Lin at the National Center for Research on Earthquake Engineering (NCREE, Taipei) for his valuable help on the experiment.

REFERENCES

[1] Achour N, Miyajima M, Kitaura M, Price A. (2011). Earthquake Induced Structural and Nonstructural Damage in Hospitals, Earthquake Spectra;27(3):617-634.

[2] Yang JN and Agrawal AK. (2000). Protective system for high-technology facilities against micro-vibration and earthquake, Structural Engineering and Mechanics;10(6):561-575.

[3] Xu YL, Yu ZF and Zhan S. (2008). Experimental study of a hybrid platform for high-tech equipment protection against earthquake and microvibration, Earthquake Engineering and Structural Dynamics ;37:747-767.

[4] Lu LY and Hsu CC. (2013). Experimental study of variable-frequency rocking bearings for seismic isolation, Engineering Structures;46(1):116-129.

[5] Lu LY, Lee TY and Yeh SW. (2011). Theory and experimental study for sliding isolators with variable curvature, Earthquake Engineering and Structural Dynamics;40(14):1609-1627.

[6] Constantinou MC, Mokha A and Reinhorn A. (1990). Teflon bearings in base isolation. II: modeling. ASCE, Journal of Structural Engineering;116:455-474.

[7] IBC (2009). International Building Code, International Code Council, Inc., Country Club Hills, Illinois, USA.